applied sciences

MDPI

Article

Strength Prediction Model for Cohesive Soil–Rock Mixture with Rock Content

Yang Sun [1], Jianyong Xin [2], Junchao He [3,*], Junping Yu [1,*], Haibin Ding [3] and Yifan Hu [3]

[1] Jiangxi Transportation Research Institute Co., Ltd., Nanchang 330200, China; 19179826061@163.com
[2] Yichun Highway Development Center Shanggao Sub-Center, Yichun 336499, China; 2023018085901026@ecjtu.edu.cn
[3] School of Civil Engineering and Construction, East China Jiaotong University, Nanchang 330013, China; hbding@ecjtu.edu.cn (H.D.); 2019011001000207@ecjtu.edu.cn (Y.H.)
* Correspondence: 18379051640@163.com (J.H.); 15779535525@163.com (J.Y.)

Abstract: Fault fracture zones, characterized by high weathering, low strength, and a high degree of fragmentation, are common adverse geological phenomena encountered in tunneling projects. This paper performed a series of large-scale triaxial compression tests on the cohesive soil–rock mixture (SRM) samples with dimensions of 500 mm × 1000 mm to investigate the influence of rock content P_{BV} (20, 40, and 60% by volume), rock orientation angle α, and confining pressure on their macro-mechanical properties. Furthermore, a triaxial numerical model, which takes into account P_{BV} and α, was constructed by means of PFC^{3D} to investigate the evolution of the mechanical properties of the cohesive SRM. The results indicated that (1) the influence of the α is significant at high confining pressures. For the sample with an α of 0°, shear failure was inhibited, and the rock blocks tended to break more easily, while the samples with an α of 30° and 60° exhibited fewer fragmentations. (2) P_{BV} significantly affected the shear behaviors of the cohesive SRM. The peak deviatoric stress of the sample with an α of 0° was minimized at lower P_{BV} (<20%), while both the deformation modulus and peak deviatoric stress were larger at high P_{BV} (>60%). Based on these findings, an equation correlating shear strength and P_{BV} was proposed under consistent α and matrix strength conditions. This equation effectively predicts the shear strength of the cohesive SRM with different P_{BV} values.

Keywords: large-scale triaxial compression test; soil–rock mixture; PFC^{3D}; strength prediction; rock content

Academic Editor: Tiago Filipe da Silva Miranda

Received: 9 December 2024
Revised: 9 January 2025
Accepted: 13 January 2025
Published: 16 January 2025

Citation: Sun, Y.; Xin, J.; He, J.; Yu, J.; Ding, H.; Hu, Y. Strength Prediction Model for Cohesive Soil–Rock Mixture with Rock Content. *Appl. Sci.* **2025**, *15*, 843. https://doi.org/10.3390/app15020843

1. Introduction

A fault fracture zone forms as a result of ruptures and misalignments of rocks due to faulting caused by crustal movement [1]. The loose rock in these fracture zones leads to low load-bearing capacity, which may lead to issues such as sinking, tilting, or even the collapse of building foundations. These fault fracture zones are predominantly soil–rock mixtures (SRMs) composed of rock blocks with relatively high strength and stiffness, as well as fault mud with low strength, which is characterized by a directional arrangement and the inclusion of large-size blocks (25–270 mm). They may lead to hazards such as landslides, toppling, uplift arch bulging, supporting structure damage, or even the overall instability of tunnel lining structure [2]. Therefore, investigating the mechanical properties of SRMs is of paramount importance.

Recent studies have predominantly focused on in situ shear tests, laboratory large-scale triaxial compression tests, and numerical simulation tests aimed at understanding the mechanical properties of SRMs in shallow landslides.

In situ tests offer advantages such as ease of implementation, lower cost, and direct access to strength parameters from in situ samples. Several scholars have conducted research on SRMs through in situ shear tests. Li et al. [3,4] and Wu et al. [5] performed several sets of in situ horizontal push-shear tests and compressive shear tests in the Baiyian landslide belt within the Three Gorges Reservoir area. They obtained the damage modes, shear deformation curves, and shear strength of SRMs under different sample sizes, force conditions, and rock contents (P_{BV}). Coli et al. [6] conducted in situ tests to derive the stress–strain curves and shear strength parameters of SRMs under different conditions. Savaly [7] carried out a series of in situ large-scale push-shear tests to examine the influence of P_{BV} on the mechanical properties of SRMs. Chandler [8] found that the shear strength of landslides substantially increases with the presence of larger sized blocks. Xu [9] et al. conducted in situ horizontal push-shear tests under natural and submerged environmental conditions to analyze the effects of parameters such as water content, P_{BV}, and grain size distribution on the shear strength index of SRMs.

In contrast to the complexities associated with in situ testing, laboratory testing allows for a more convenient and systematic exploration of the mechanical behaviors of SRMs under varying factors. Kalender et al. [10] prepared an artificial SRM within a test chamber and performed uniaxial and triaxial tests. Vallejo et al. [11,12] explored the effect of P_{BV} on the shear strength and internal void ratios of SRMs, and found that the shear strength of SRMs is largely determined by the degree of aggregation between the stones and soil. Kuenza et al. [13] conducted undrained shear tests and concluded that the strain softening characteristics of the samples were positively correlated with the gravel content. Bagherzadeh-Khalkhali et al. [14] analyzed the mechanical properties of coarse-grained soils with different particle sizes and particle gradations. The results showed that the internal friction angle and the degree of shear expansion increased with increasing particle size. Vallejo et al. [11] and Jalili et al. [15] investigated the effect of factors such as P_{BV}, the grading of SRM on its shear strength, deformation mechanism, and shear damage characteristics through laboratory large-scale direct shear tests. Cao et al. [16] studied the effect of P_{BV} on the deformation and strength of SRMs using a specially designed large-scale lateral limit consolidator for airport fill in the western mountainous area.

However, technical challenges often arise during sample preparation for laboratory testing, which necessitates the use of numerical simulation as effective complements. You et al. [17] employed the finite-difference software FLAC to model blocks as regular polygons (e.g., circles, squares, and triangles) to establish a two-dimensional stochastic fine structure model for SRMs and carried out a series of uniaxial compression numerical tests. Kenoko et al. [18] analyzed the development of shear zones in granular geotechnical materials subjected to shear using the numerical tests that integrated discrete and finite methods. Liu et al. [19] established a finite element model for rainfall infiltration on SRM slopes, and analyzed unstable rainfall infiltration scenarios in both homogeneous and inhomogeneous media. Zhang utilized FLAC to model SRMs as two-phase composites consisting of rock blocks and a soil matrix. Hadjigeorgiou et al. [20] investigated the stability of SRMs during excavation by integrating a 3D fracture system model into discrete element software PFC^{3D} (V-3.0). Fakhimi [21] developed a hybrid DEM/FEM model to study the mechanical behaviors of geotechnical materials, where the soil or rock mass was treated as a system of discrete spheres. Bian et al. [22] simulated the deformation characteristics of SRMs under different temperatures using the $FLAC^{3D}$ (v.2.10), and analyzed the effect of temperature on pore water pressure, deformation, and displacement. Lee et al. [23] conducted numerical drained and undrained triaxial compression tests under different confining pressures and initial porosities using discrete element polyhedral cells.

In summary, extensive research on in situ shear tests, laboratory large-scale triaxial compression tests, and numerical simulations concerning the mechanical properties of SRMs has been conducted, yielding results that can provide valuable guidance for practical engineering applications. Nonetheless, notable deficiencies remain in the study of SRMs within fault fracture zones:

(1) There are few current studies into SRMs in deep fault fracture zones, where sampling poses significant challenges, necessitating alternative materials to simulate fault mud.
(2) Standard large triaxial compression testing machines introduce size effects on SRMs in fault fracture zones with block sizes of 25–270 mm [24,25]; therefore, large triaxial compression tests are required to assess the impact of sample size on the mechanical properties of SRMs, thereby mitigating the influence of size effects.
(3) The limited number of laboratory triaxial compression tests prevents generalization to fault fracture zones comprising various fault mud types and different P_{BV} values in SRMs. The use of the discrete element technique allows for the reproduction of laboratory triaxial compression tests for SRMs, the calibration of interaction models and mechanical parameters between the rock block and the soil matrix, and the analysis of influencing factors, which can be extended to a wider range of SRMs.

To address these issues, this study conducted laboratory large-scale triaxial compression tests on SRM samples with dimensions of 500 × 1000 mm to investigate the effects of confining pressure, P_{BV}, and α on their mechanical properties. Subsequently, a numerical model considering P_{BV} and α was established using discrete element software PFC^{3D} (v.6.0) to facilitate the microsimulation study of the cohesive SRM. Finally, a strength prediction model was derived for the cohesive SRM based on P_{BV}.

2. Test Materials

2.1. Materials and Methods

In this study, a bentonite–cement mixture and high-calcium limestone were selected to simulate cohesive fault mud and rock blocks, respectively. The target strength of cohesive fault mud was achieved by adjusting the mixing ratios of bentonite, cement, and water. The sample preparation method was as follows: first, a layer of mixture was added. Immediately after that, the blocks were added and again the mixture was added to achieve self-compaction by gravity. The cycle was repeated five times until the sample preparation cylinder was filled. Bentonite–cement pastes with different mixing ratios were prepared in accordance with the concrete mixing ratio design (see in Figure 1), and the shear strength of the bentonite–cement pastes was determined by averaging the results from three sets of parallel tests for each specified mixing ratio. The shear strength of the bentonite–cement pastes under different mixing ratios is listed in Table 1. The result is compared through Figure 2.

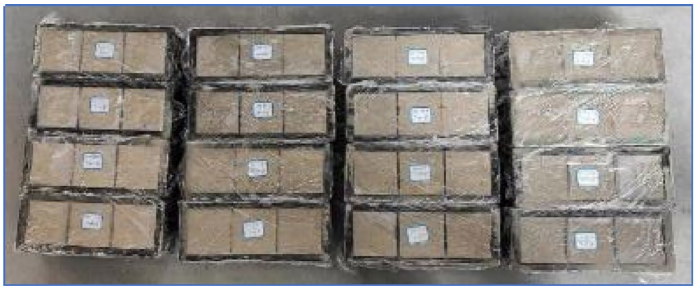

Figure 1. Artificial fault mud sample.

Table 1. Undrained shear strength of cohesive fault mud with different ratios.

Number	Water (kg)	Bentonite (kg)	Cement (kg)	Shear Strength (kPa)
a	10	1	2	<10
b			3	38.65
c			4	40.35
d		1.5	2	33.52
e			3	51.35
f			4	65.72
g		2	2	42.74
h			3	61.84
i			4	84.82

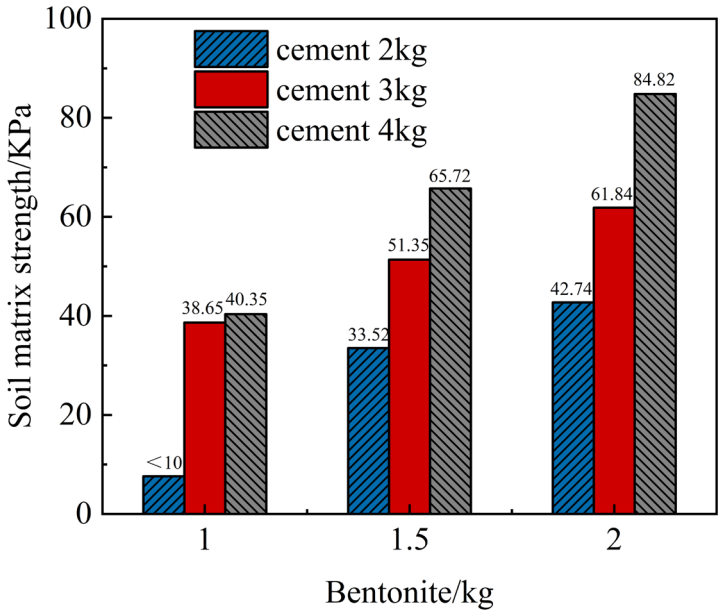

Figure 2. Undrained shear strength of cohesive fault mud with different ratios.

2.2. Analysis of Material Proportioning Results

The results indicated that as water content increased, the matrix strength of the bentonite–cement pastes initially rose and subsequently declined, which suggested the existence of an optimal water content that maximized matrix strength. This phenomenon could be attributed to two factors: when the water content was too low, the cement paste was inadequately hydrated, resulting in the insufficient cementation of the soil; when the water content was too high, the strength of the cement paste decreased, weakening the soil's cementing effect. With the increase in bentonite dosage, the matrix strength of the bentonite–cement pastes showed a tendency of first increasing and then decreasing, thus indicating the presence of an optimal bentonite dosage for maximizing matrix strength.

The effects of different water-to-bentonite (W/B) ratios on the fluidity and stability of the matrix are depicted in Figure 3. A W/B ratio of 1:0.1 required the matrix to cure for five days before achieving a gel suitable for holding the rock blocks, which indicated that the fluidity of the matrix was too low for use. A W/B ratio of 1:0.15 resulted in excessive fluidity, as the matrix failed to adequately hold rock blocks even after one-day curing, which indicated that the stability of the matrix was too poor for use. At a W/B ratio of 1:0.2, the matrix exhibited excellent fluidity and stability after one-day curing, while rock blocks could be held efficiently, which indicated that the performance of the matrix at this W/B ratio was more suitable for testing. When the W/B ratio was 1:0.33, the matrix displayed

extremely high viscosity during mixing, while rock blocks could be placed directly, which indicated that the matrix was very expansive but too viscous for use.

W:B = 1:0.1 W:B = 1:0.15 W:B = 1:0.2 W:B = 1:0.33

Figure 3. Artificial fault mud bentonite matrix sample.

2.3. Determination of Test Materials

This study conducted large-scale triaxial compression tests using a matrix mixture with a mixing ratio of W:B:C = 1:0.2:0.4, which had been cured for one day. Prior to sample preparation, bentonite–cement pastes with different mixing ratios (see Figure 4) were extracted and subjected to conventional triaxial compression tests, as shown in Figure 5.

400 kPa 800 kPa 1600 kPa

Figure 4. Soil matrix damage pattern.

Figure 5. GSZ501 large triaxial compression tester for coarse-grained soil (size sample of Φ500 × 1000 mm).

Figure 6 presents the stress–strain curves corresponding to various confining pressures at a P_{BV} of 40%.

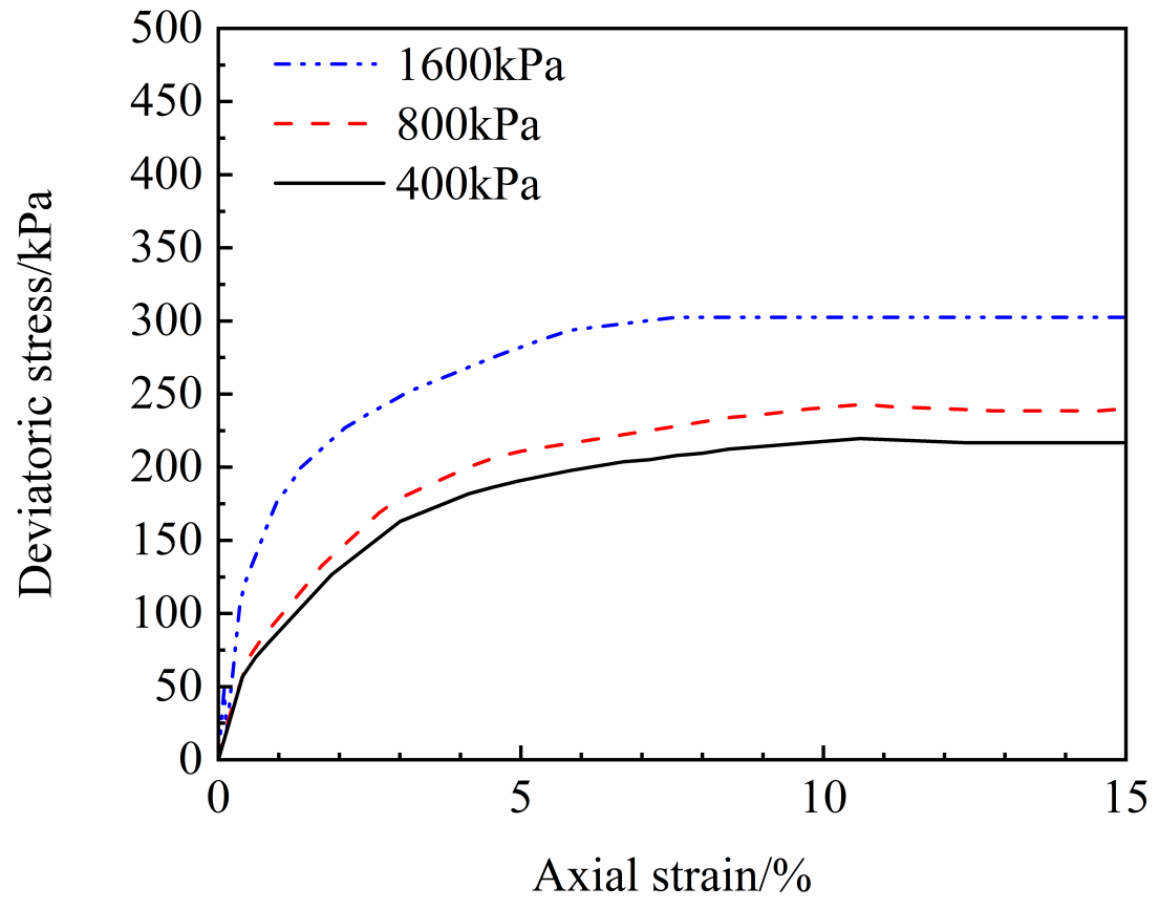

Figure 6. Stress–strain curves at a P_{BV} of 40%.

3. Analysis of Large-Scale Triaxial Compression Test Results of Cohesive SRM

3.1. Effect of P_{BV} on Cohesive SRM

Figure 7 illustrates the deviatoric stress–axial strain curves of samples with different P_{BV} values at a constant confining pressure. At lower P_{BV} values of 0, 20, and 40%, the curve exhibited a slow increase, whereas at a higher P_{BV} value of 60%, a significant increase was identified. The shape of the curves indicated that the cohesive SRM samples demonstrate weak softening characteristics. Due to a series of problems such as the violent occlusion collision between the internal blocks during the loading process of the SRM sample with a P_{BV} of 0.6 and a block inclination angle of 60°, it is often difficult to carry out the test.

At low P_{BV} values, the strain curves of the samples with low relative matrix compactness displayed strain hardening (or weak softening) when they were loaded. However, the loading curves of the samples exhibited a softening trend when the P_{BV} values reached 0.4 and above. Under high P_{BV} conditions, the properties of the cohesive SRM samples were mainly determined by the rock blocks. At this time, the stones bite each other to form a skeleton structure, and the soil matrix mainly fills the pores. With the further increase in P_{BV}, the proportion of soil matrix decreases, and its influence on the SRM samples becomes less and less.

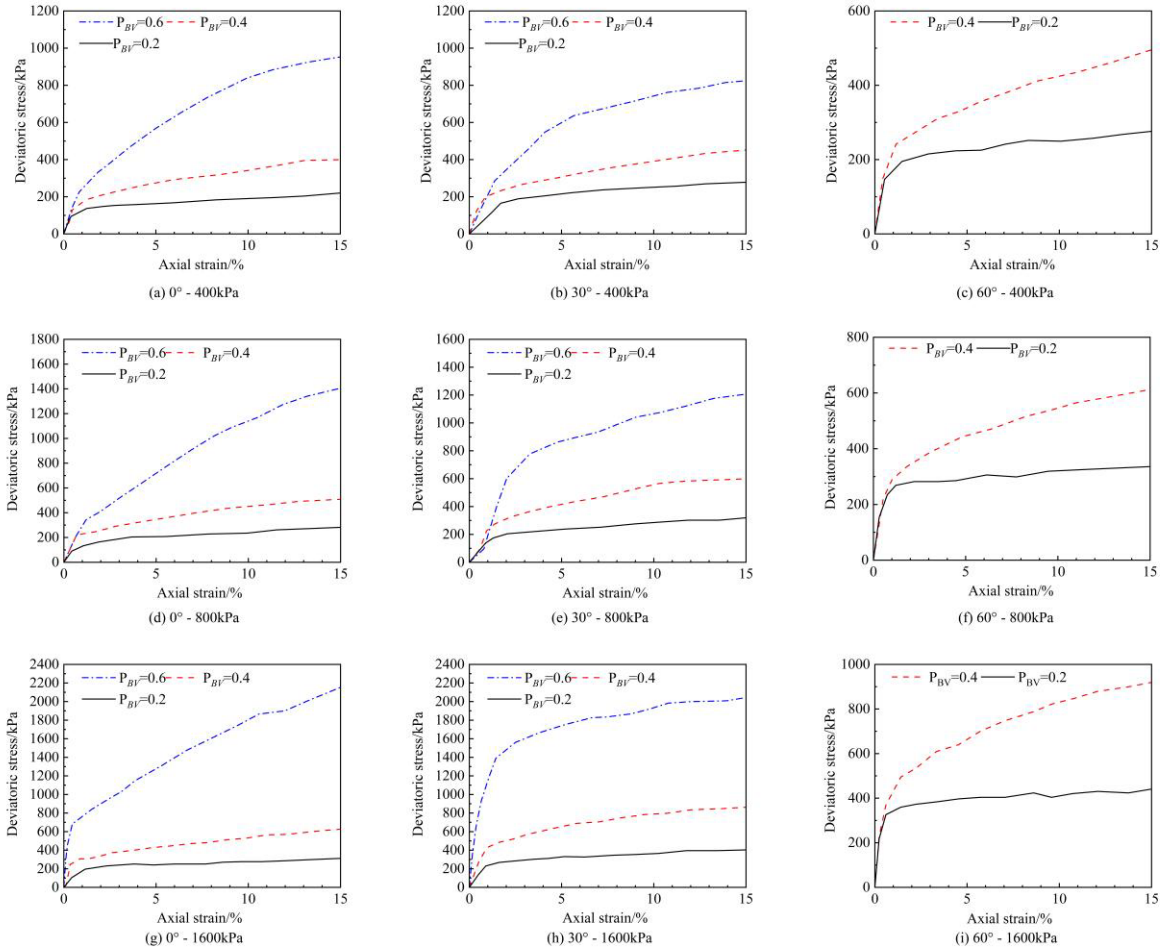

Figure 7. Stress-strain curves for samples with different P_{BV} values.

3.2. Shear Strength of Cohesive SRM

Figure 8 depicts the strength curves of cohesive SRM samples under different confining pressures and P_{BV} values. The results indicated that, under constant confining pressure, the shear strength of the samples increased with increasing P_{BV}. At lower P_{BV} values (20% < P_{BV} < 40%), the growth of the curves was moderate; however, at higher P_{BV} values (40% < P_{BV} < 60%), a significant increase in the curves was observed. This phenomenon was attributed to the fact that, at lower P_{BV} values, the SRM was predominantly composed of cohesive soil with a limited number of rock blocks. In this case, the mixture structure was looser, and the rock blocks remained dispersed within the cohesive soil, thus failing to form an effective skeleton structure. The mechanical properties of cohesive soils play an important role at this stage. However, the shear strength of cohesive soil was relatively low and varied more gently. Therefore, at lower P_{BV} values, adding small amounts of rock blocks did not significantly enhance the overall shear strength, resulting in a flatter increase in the curve. As P_{BV} increased, the number of rock blocks also increased, gradually forming a skeleton structure. This skeleton structure effectively bore the external loads and improved the overall stability of the mixture. The increased mutual contact and occlusion between the rock blocks allowed the SRM to better transfer stresses when subjected to shear forces, thereby increasing the shear strength. As a result, the growth of the curve became significantly pronounced.

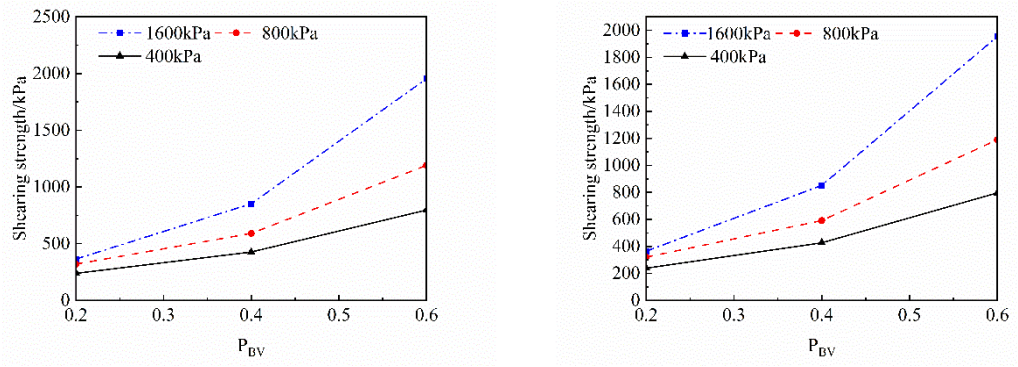

(**a**) $\alpha = 0°$ (**b**) $\alpha = 30°$

Figure 8. Relationship curve between P_{BV} and shear strength.

4. Numerical Simulation on Mechanical Properties of Cohesive SRM

4.1. Modeling

The discrete element numerical simulation in this study was based on the PFC^{3D} software, which is mainly employed to simulate bulk particles or systems that can be simplified to bulk particles. In PFC^{3D} software, spherical particles serve as the basic modeling units. These spherical particles represent the corresponding particle gradation of the tested soil material and can be bonded to simulate the solid material, such as the rock blocks in this study. The model employs walls to establish boundaries, and the contact forces arise from the overlapping interactions between particles and between particles and walls. Based on the experimental results, the most suitable intrinsic model is selected for the existing program of PFC^{3D}. Given the relative simplicity and high computational efficiency of the linear contact model, which can significantly reduce the computational time and resource consumption in the large-scale simulation or complex engineering analysis of cohesive SRMs, this study adopted the linear contact model. Since walls in PFC^{3D} cannot be directly loaded with stress, the constant confining pressure applied to the sample needs to be achieved by adjusting the wall velocity through a numerical servo mechanism.

For clay particles, PFC^{3D} controls the number of particles mainly by adjusting the porosity. The relationship is as follows Equations (1) and (2). e is the matrix porosity ratio; e_{max} is the matrix maximum porosity ratio; e_{min} is the matrix minimum porosity ratio; Dr is the matrix relative compactness. In this test, Dr = 0.3 and n = 0.43, which are dimensionless. For the blocks, this study designs an R_{block} rectangular block template with a length-to-width-to-height ratio of 2:1:1. The long axis of R_{block} can be controlled to be 8 mm. In this paper, the flexible particle film servo method is selected, in order to ensure that the specimen is subjected to a stable lateral pressure, and the servo control system of the PFC software must be used to precisely regulate the speed of the wall movement in order to achieve the predetermined lateral pressure. In this study, five different loading rates were chosen, i.e., 0.25, 0.20, 0.15, 0.10, and 0.05 m/s. In order to balance the model computational accuracy and computational time, a loading rate of 0.15 m/s was chosen for simulation in this model (Da Cruz F et al., 2005) [26]. The parameters related to numerical modeling are shown in Table 2.

$$e = e_{max} - (e_{max} - e_{min}) \tag{1}$$

$$n = \frac{e}{1+e} \tag{2}$$

Table 2. Table of model parameters.

Relative Density of the Matrix	Block Length-to-Width-to-Height Ratio	The Long Axis of R_{block}	Loading Rate
Dr = 0.3	2:1:1	8 mm	0.15 m/s

This study developed a flexible triaxial compression numerical model of the cohesive SRM with 40% P_{BV} and an α of 30° using PFC^{3D} software. The model was calibrated through the laboratory large-scale triaxial compression test results, and the calibrated micro-mechanical parameters for the cohesive SRM samples are summarized in Table 3. As revealed in Figures 9 and 10, the deviatoric stress versus axial strain curves and the failure modes of the samples obtained from the numerical tests were largely consistent with the laboratory test results. These observations confirmed the validity of the numerical model presented in this study.

Table 3. Meso-scale mechanical parameters for the cohesive SRM samples.

	Density	Contact Stiffness (N/m)		Bonding Strength (N)		Frictional Coefficient
	(kg/m^3)	normal	tangential	normal	tangential	
soil mass	1920	5.0×10^6	2.0×10^6	3.0×10^2	3.0×10^2	
block	2890	1.0×10^8	1.0×10^8	-	-	1
soil mass block	-	4.8×10^6	1.9×10^6	0	0	0.45
film	1500	7.0×10^6	4.7×10^6	1.0×10^{300}	1.0×10^{300}	0

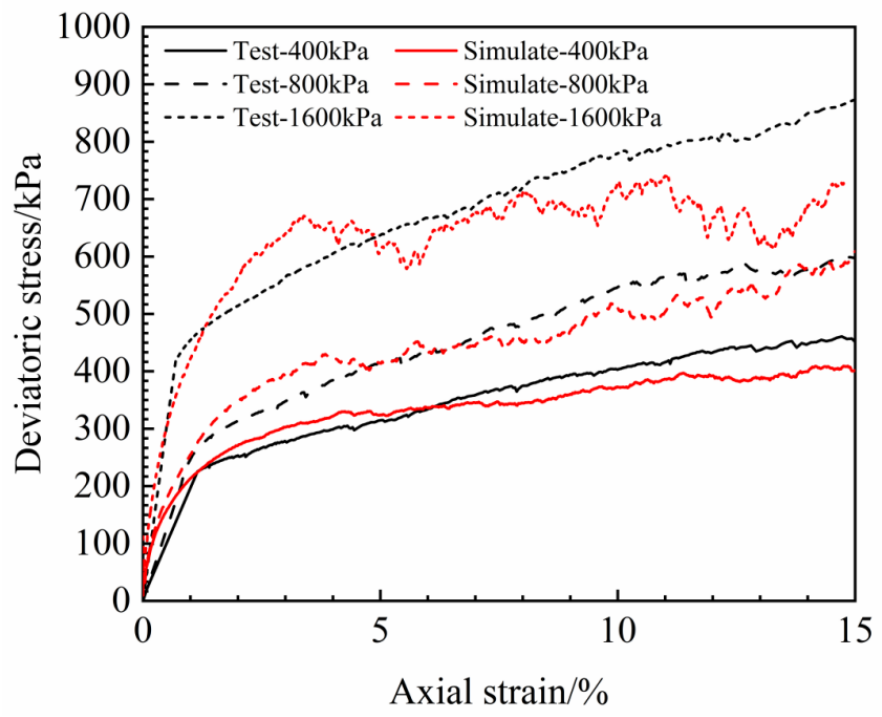

Figure 9. Calibration results.

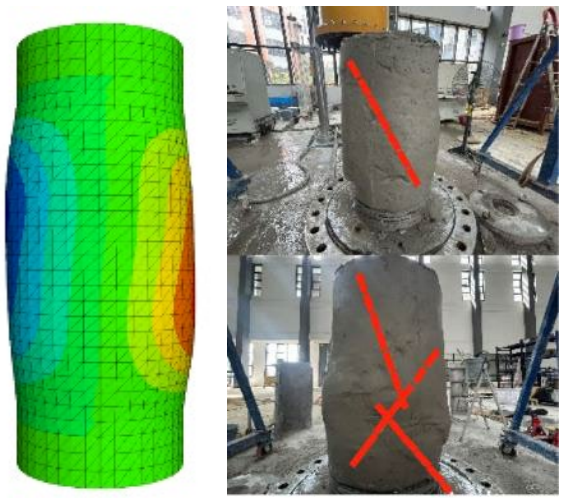

Figure 10. Failure modes.

4.2. Stress–Strain Curves for Samples with Different P_{BV} Values

The cohesive SRM samples were subjected to a confining pressure of 400 kPa, and the shear strength versus axial strain curves for different P_{BV} values were recorded, as illustrated in Figure 11.

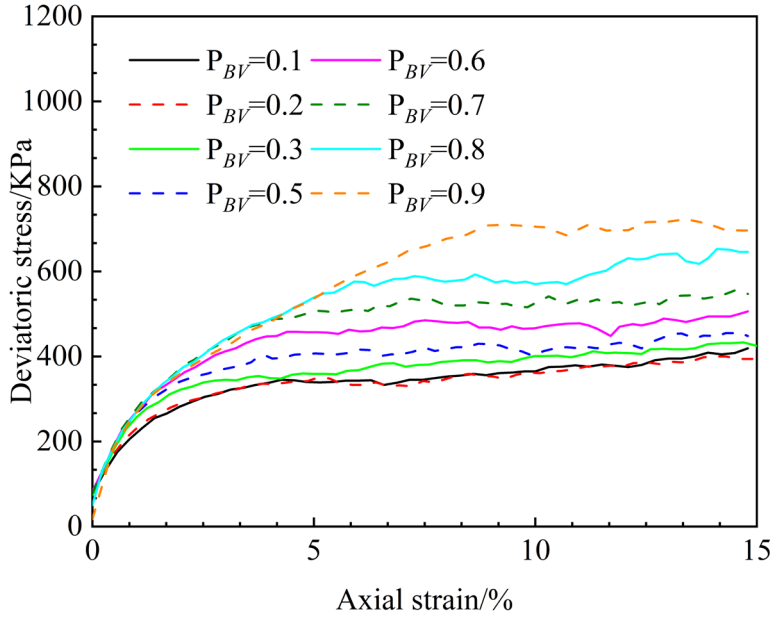

Figure 11. Simulated stress–strain curves of the cohesive SRM at a confining pressure of 400 kPa.

The simulated stress–strain curves of the cohesive SRM sample at a confining pressure of 400 kPa were used as an example for study. It was revealed that P_{BV} significantly influenced the shear behaviors of the SRM. Specifically, when P_{BV} did not exceed 20%, the curves nearly overlapped, and the properties were dominated by the viscous matrix. Conversely, when P_{BV} exceeded 20%, the peak deviatoric stress increased proportionally with P_{BV}. Furthermore, as P_{BV} rose, the initial slope of the curves also increased, which demonstrated an enhanced modulus of deformation and a greater achievable peak deviatoric stress. When P_{BV} was 70% and above, stress jumps were observed in local curves, which could be attributed to the formation of large internal voids due to high P_{BV}. During the compression process, sudden unloading could occur from stone to stone, leading to structural reorganization.

4.3. Prediction Method for Shear Strength of Cohesive SRM

Figure 11 illustrates the shear strength versus axial strain curves for cohesive SRM samples with different P_{BV} values at a confining pressure of 400 kPa. Figure 12 presents a scatter plot illustrating the relationship between P_{BV} and shear strength.

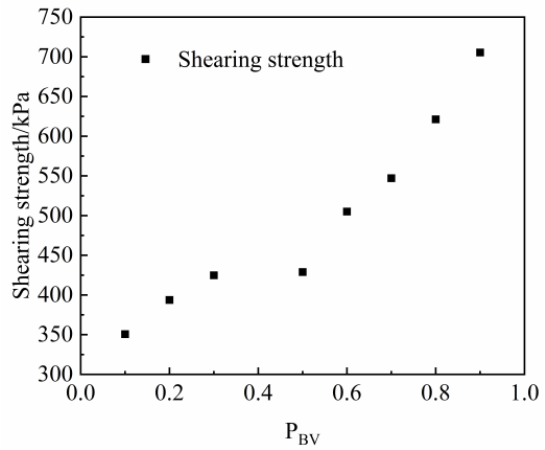

Figure 12. Scatter plot of P_{BV} vs. shear strength.

As shown in Figure 13, based on the scatter plot trend fitting curve, its growth trend follows a logistic function.

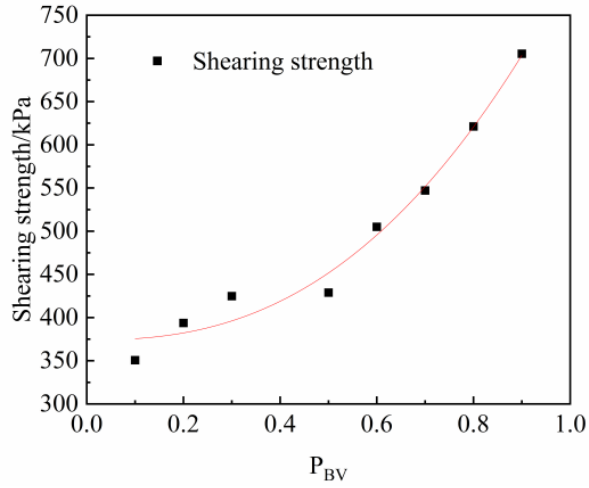

Figure 13. Fitted graph.

According to Figure 13, the relationship between P_{BV} and shear strength can be expressed by the following formula (Equation (3)):

$$\tau = A + \frac{B - A}{1 + \left(\frac{P_{BV}}{C}\right)^{D}} \quad (3)$$

where B denotes the shear strength when $P_{BV} = 0$, defined as τ_0, where three linearly independent parameters A, C, and D exist.

For the logistic function, the rapidly increasing portion is governed by two parameters, C and D, where D plays a dominant role and B plays a secondary role. Previous studies on SRMs have identified key P_{BV} thresholds for shear strength at 0.2–0.3 and 0.7–0.8 [10]. Therefore, the expected thresholds were approached by controlling parameters C and D based on the test results. Thus, parameters C and D were determined to be 25 and 2.4,

respectively. The goodness of fit of the fitted curve, $R^2 = 0.978$, indicates that the fit of the curve is applicable.

$$\tau = A + \frac{\tau_0 - A}{1 + \left(\frac{P_{BV}}{25}\right)^{2.4}} \quad (4)$$

where A is the single unknown variable. Therefore, for a given shear strength of a cohesive SRM at any P_{BV}, the specific relationship between shear strength and P_{BV} can be determined from Equation (4).

4.4. Validation of Strength Prediction Formulas for Cohesive SRM

Based on the above analysis of the strength parameters of the cohesive SRM, the magnitude of the parameter A value in Equation (4) is further adjusted, and when $A = 10^6$, the relationship curve between P_{BV} and shear strength is obtained as shown in Figure 14.

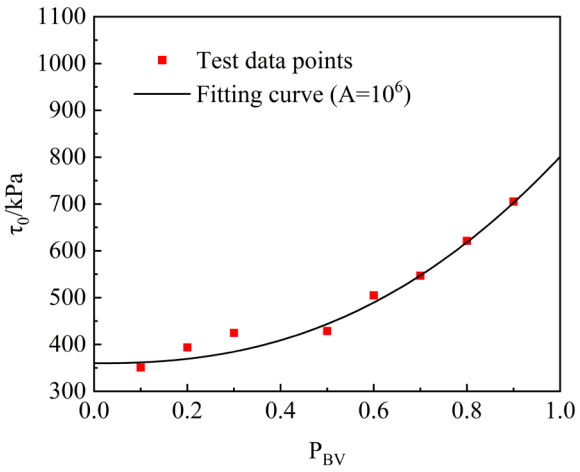

Figure 14. Relationship curve between P_{BV} and shear strength.

Figure 14 clearly demonstrates that both experimental and numerical data coincide with the theoretical curve. Consequently, Equation (4) can be used to better reflect the relationship between the P_{BV} and shear strength of the SRM.

5. Conclusions

In this study, cohesive SRM samples were prepared using high-strength matrix as the soil matrix and high-calcium limestone as the block material. Given the excellent water absorption properties of bentonite, it is essential to allow adequate time for bentonite to fully absorb water and expand, thereby forming a suspended and gelled state that optimally utilizes its properties. The curing time for the matrix varied depending on the W/B ratio.

(1) The shear strength and modulus of elasticity of the cohesive SRM samples increased with increasing P_{BV}. P_{BV} significantly influenced the shear damage characteristics of the cohesive SRM, and the shear behaviors of the cohesive SRM with low P_{BV} were similar to those of its matrix soil. When P_{BV} reached a high level, the shear damage of the cohesive SRM exhibited pronounced softening characteristics, accompanied by a significant shear expansion phenomenon.

(2) A numerical model of the cohesive SRM was established using PFC^{3D} to further analyze the effects of P_{BV} and α on its macroscopic mechanical properties. The results showed that the strength of the samples first decreased and then increased as α increased from 0° to 90° at a fixed P_{BV}. When P_{BV} was low, the blocks uniformly distributed within the cohesive SRM could bear the external loads, thereby enhancing the rock's resistance to damage. When P_{BV} was too high, it led to an increase in the contact between the blocks, resulting in a relatively weakened bonding effect of the cohesive SRM. In this case, the rock

was prone to stress concentrations which occurred in the block contact area, which reduced the overall strength.

(3) The relationship between the P_{BV} and shear strength of the cohesive SRM can be described by the equation $\tau = A + \frac{\tau_0 - A}{1 + \left(\frac{P_{BV}}{25}\right)^{2.4}}$. This formula facilitates the strength prediction for the cohesive SRM with different P_{BV} values.

The limitation of this work only concerns the relationship between the shear strength of the cohesive SRM and the amount of stone content, and it is difficult to study the relationship between the shear strength of the SRM and the block inclination due to the difficulty of controlling the block inclination of the cohesive SRM in the experiments. Future efforts will be devoted to the further study of block inclination.

Author Contributions: Conceptualization, Y.S. and J.X.; Methodology, Y.S. and H.D.; Validation, Y.S. and J.X.; Investigation, H.D.; Visualization, Y.S., J.X. and J.H., J.Y. and Y.H.; Supervision, J.H. and H.D. All authors have read and agreed to the published version of the manuscript.

Funding: This research was supported by the Science and Technology Project Fund of Jiangxi Provincial Department of Transportation (2022Z0001 and 2022Z0002).

Institutional Review Board Statement: Not applicable.

Informed Consent Statement: Not applicable.

Data Availability Statement: Data is not available due to privacy and ethical restrictions.

Conflicts of Interest: Authors Yang Sun and Junping Yu were employed by the company Jiangxi Transportation Research Institute Co., Ltd. The remaining authors declare that the research was conducted in the absence of any commercial or financial relationships that could be construed as a potential conflict of interest. The authors declare no conflicts of interest.

References

1. Medley, E.; Goodman, R.E. Estimating the block volumetric proportions of melanges and similar block in-matrix rocks (bimrocks). In Proceedings of the 1st North American Rock Mechanics Symposium, Austin, TX, USA, 1–3 June 1994; American Rock Mechanics Association: Seattle, WA, USA, 1994.
2. Dearman, W.R. Description and Classification of Weathered Rocks for Engineering Purposes-the Background to the B55930-1981 Proposals. *Q. J. Eng. Geol.* **1995**, *28*, 267–276. [CrossRef]
3. Li, X.; Liao, Q.L.; He, J.M. In-situ tests and a stochastic structural model of rock and soil aggregate in the three gorges reservoir area, china. *J. Rock Mech. Min. Sci.* **2005**, *41*, 494–495. [CrossRef]
4. Li, X.; Liao, Q.L.; He, J.M. Study on in-situ tests of mechanical characteristics on soil-rock aggregate. *J. Rock Mech. Eng.* **2007**, *26*, 2377–2384. (In Chinese)
5. Liao, Q.L.; Li, X.; Hao, Z.; Wang, S.; Wu, M.; He, J. Current status and future trends of studies on rock and soil aggregates. *J. Eng. Geol.* **2006**, *14*, 800–807. (In Chinese)
6. Coli, N.; Berry, P.; Boldini, D. In situ non-conventional shear tests for the mechanical characterisation of a bimrock. *Int. J. Rock Mech. Min. Sci.* **2011**, *48*, 95–102. [CrossRef]
7. Savaly, J.P. Determination of shear strength of conglomerates using a caterpillar D9 ripper and comparsion with alternative methods. *Int. J. Min. Geol. Eng.* **1990**, *8*, 203–225. [CrossRef]
8. Chandler, R.J. Inclination of talus, arctic talus terraces, and other slopes composed of granular materials. *J. Geol.* **1973**, *8*, 1–14. [CrossRef]
9. Xu, W.J.; Hu, R.L.; Tan, R.J. Some geomechanical properties of SRMs in Tiger-Leaping Gprge Area, China. *China Geotech.* **2007**, *57*, 255–264. [CrossRef]
10. Kalender, A.Y.C.A.N.; Sonmez, H.; Medley, E.; Tunusluoglu, C.; Kasapoglu, K.E. An approach to predicting the overall strengths of unwelded bimrocks and bimsoils. *Eng. Geol.* **2014**, *183*, 65–79. [CrossRef]
11. Vallejo, L.E.; Mawby, R. Porosity influence on the shear strength of granular material-clay mixtures. *Eng. Geol.* **2000**, *58*, 125–136. [CrossRef]
12. Vallejo, L.E. Interpretation of the limits in shear strength in binary granular mixtures. *Can. Geotech. J.* **2001**, *38*, 1097–1104. [CrossRef]

13. Kuenza, K.; Towhata, I.; Orense, R.P.; Wassan, T.H. Undrained torsional shear tests on gravelly soils. *Landslides* **2004**, *1*, 185–194. [CrossRef]
14. Bagherzadeh-Khalkhali, A.; Mirghasemi, A.A. Numerical and experimental direct shear tests for coarse-grained soils. *Particuology* **2009**, *7*, 83–91. [CrossRef]
15. Jalili, J.; Jafari, M.K.; Shafiee, A.; Koseki, J.; Sato, T. An investigation on effect of inclusions on heterogeneity of excess pore pressure and strain distribution in composite soils. *Int. J. Civ. Eng.* **2012**, *10*, 124–138.
16. Cao, G.X.; Xu, M.; Song, E.X. Mechanic properties of broken rock-soil mixture. *J. South China Univ. Technol. (Nat. Sci. Ed.)* **2010**, *38*, 32–39. (In Chinese)
17. You, X.H. Stochastic structural Model of the earth-rock aggregate and its application. *J. Rock Mech. Eng.* **2002**, *11*, 1748. (In Chinese)
18. Kaneko, K.; Terada, K.; Kyoya, T.; Kishino, Y. Global–local analysis of granular media in quasi-static equilibrium. *Int. J. Solids Struct.* **2003**, *40*, 4043–4069. [CrossRef]
19. Liu, Y.; Liu, Q.; Chen, H.; Gong, X.; Zhang, D.; Yao, D.; Li, L. Numerical study on rainfall infiltration in rock-soil slop. *Sci. China (Ser. E Technol. Sci.)* **2005**, *48*, 33–46. [CrossRef]
20. Hadjigeorgiou, J.; Esmaieli, K.; Grenon, M. Stability analysis of vertical excavations in hard rock by integrating a fracture system into a PFC model. *Tunn. Undergr. Space Technol.* **2009**, *24*, 296–308. [CrossRef]
21. Fakhimi, A. A hybrid discrete–finite element model for numerical simulation of geomaterials. *Comput. Geotech.* **2009**, *36*, 386–395. [CrossRef]
22. Bian, H.B.; Jia, Y.; Armand, G.; Duveau, G.; Shao, J.F. 3D numerical modelling thermo-hydromechanical behaviour of underground storages in clay rock. *Tunn. Undergr. Space Technol.* **2012**, *30*, 93–109. [CrossRef]
23. Lee, S.J.; Hashash, Y.; Nezami, E.G. Simulation of triaxial compression tests with polyhedral discrete elements. *Comput. Geotech.* **2012**, *43*, 92–100. [CrossRef]
24. Yoshinaka, R.; Osada, M.; Park, H.; Sasaki, T.; Sasaki, K. Practical determination of mechanical design parameters of intact rock considering scale effect. *Eng. Geol.* **2008**, *96*, 173–186. [CrossRef]
25. Lin, Z.; Jiang, Y.; Xiong, Y.; Xu, C.; Guo, Y.; Wang, C.; Fang, T. Analytical solution for displacement-dependent active earth pressure considering the stiffness of cantilever retaining structure in cohesionless soil. *Comput. Geotech.* **2024**, *170*, 106258. [CrossRef]
26. Da Cruz, F.; Emam, S.; Prochnow, M.; Roux, J.N.; Chevoir, F. Rheophysics of dense granular materials: Discrete simulation of plane shear flows. *Phys. Rev. E Stat. Nonlinear Soft Matter Phys.* **2005**, *72*, 021309. [CrossRef] [PubMed]